# Weak and Strong Constraints Variational Data Assimilation with the NCOM-4DVAR in the Agulhas Region Using the Representer Method

HANS NGODOCK, MATTHEW CARRIER, AND SCOTT SMITH

*Naval Research Laboratory, Stennis Space Center, Mississippi*

INNOCENT SOUOPGUI

*Department of Marine Sciences, University of Southern Mississippi, Stennis Space Center, Mississippi*

(Manuscript received 12 July 2016, in final form 18 January 2017)

ABSTRACT

The difference between the strong and weak constraints four-dimensional variational (4DVAR) analyses is examined using the representer method formulation, which expresses the analysis as the sum of a first guess and a finite linear combination of representer functions. The latter are computed analytically for a single observation under both strong and weak constraints assumptions. Even though the strong constraints representer coefficients are different from their weak constraints counterparts, that difference is unable to help the strong constraints compensate for the loss of information that the weak constraints includes. Numerical experiments carried out in the Agulhas retroflection for single and multiobservation assimilations clearly show that the weak constraint 4DVAR produces analyses that fit the observations with significantly higher accuracy than the strong constraints.

## 1. Introduction

The majority of applications of the four-dimensional variational data assimilation (4DVAR) use the strong constraints approach [e.g., the list of references in Di Lorenzo et al. (2007)], which assumes that errors are confined to the initial state of the model. This is true for purely deterministic problems. In most systems and applications however, especially in meteorology and oceanography, errors also arise from empirical parameterization, unresolved processes, inadequate resolution, and forcing. From the initial works of Le Dimet and Talagrand (1986), strong constraints 4DVAR gained popularity in the 1990s, particularly in the meteorological data assimilation community [e.g., the many applications of the incremental 4DVAR introduced by Courtier et al. (1994)]. One of the reasons strong constraint 4DVAR gained more popularity than the weak constraints is the technical difficulty associated with solving the normal equation for the minimization of the cost function. The process requires the inversion of all the error covariances involved: the background and the observations error covariances for the strong constraints, and the weak constraints also involves the model error covariance. It is not only difficult to prescribe a model error covariance, but also its inversion poses a significant computational challenge. Fortunately, the representer method of Bennett (1992) formulates the 4DVAR problem in such a way that the solution procedure involves only covariance multiplications, and not their inverses, with variables defined in the state and observations spaces. Nonetheless, strong constraints 4DVAR works well in cases where a relatively short assimilation window is considered so as to inhibit the growth of initial conditions errors or errors from other sources.

When compared to the strong constraints method, the weak constraints assimilation has always yielded more accurate results. This is due to the higher number of degrees of freedom in the weak constraints approach (e.g., Zupanski 1997; Vidard et al. 2004; Di Lorenzo et al. 2007). Lindskog et al. (2009) also found a similar result for an atmospheric model, even with a model error covariance that needed improvements, according to the authors. This paper attempts to

Naval Research Laboratory Contribution Number NRL/JA/7320-16-3099.

*Corresponding author e-mail*: Hans.Ngodock@nrlssc.navy.mil

DOI: 10.1175/MWR-D-16-0264.1

illustrate the fundamental difference between the two methods by quantifying the additional correction that is neglected when the strong constraints approach is adopted, using the framework of the representer method, Bennett (1992, 2002). The next section reviews the formulation of the 4DVAR problem with the representer method and derives the analytical solution of a representer function in both strong and weak constraints. Section 3 consists of numerical experiments, followed by a discussion in section 4, and conclusions in section 5.

## 2. The 4DVAR system

Consider a model described by the following equations:

$$\begin{cases} \dfrac{\partial \mathbf{u}}{\partial t} = \mathbf{L}(\mathbf{u}) + \mathbf{F} + \mathbf{f}, & 0 \le t \le T, \\ \mathbf{u}(\mathbf{x}, 0) = \mathbf{I}(\mathbf{x}) + \mathbf{i}(\mathbf{x}), \end{cases} \tag{1}$$

where $\mathbf{u}(\mathbf{x}, t)$ represents the state of the modeled phenomenon at a given time, $\mathbf{L}$ represents the dynamics and physics that are nonlinear in nature, $\mathbf{F}(\mathbf{x}, t)$ is a forcing term and $\mathbf{f}(\mathbf{x}, t)$ is a model error that can arise from different sources and has a covariance $\mathbf{C}_f$, $\mathbf{I}$ is the initial condition, and $\mathbf{i}$ is the error in the initial condition with covariance $\mathbf{C}_i$,. Let us also consider a vector $\mathbf{Y}$ of $M$ observations in the space–time domain, with the associated vector of observation errors $\boldsymbol{\varepsilon}$ (with covariance $\mathbf{C}_\varepsilon$,),

$$\mathbf{y}_m = \mathbf{H}_m \mathbf{u}(\mathbf{x}, t_m) + \boldsymbol{\varepsilon}_m, \quad 1 \le m \le M, \tag{2}$$

where $\mathbf{H}_m$ is the observation operator associated with the $m$th observation, which transforms the model solution into observation equivalents. We have assumed in (2) that the observations are sampled at some model times, thus $\mathbf{H}_m$ acts on the spatial dimensions of the solution. One can define a weighted cost function,

$$J = \int_0^T \int_\Omega \int_0^T \int_\Omega \mathbf{f}(\mathbf{x}, t) \mathbf{W}_f(\mathbf{x}, t, \mathbf{x}', t') \mathbf{f}(\mathbf{x}', t')\, d\mathbf{x}'\, dt'\, d\mathbf{x}\, dt + \int_\Omega \int_\Omega \mathbf{i}(\mathbf{x}) \mathbf{W}_i(\mathbf{x}, \mathbf{x}') \mathbf{i}(\mathbf{x}')\, d\mathbf{x}'\, d\mathbf{x} + \boldsymbol{\varepsilon}^{\mathrm{T}} \mathbf{W}_\varepsilon \boldsymbol{\varepsilon}, \tag{3}$$

where $\Omega$ denotes the spatial domain, the weights $\mathbf{W}_f$ and $\mathbf{W}_i$ are defined as inverses of $\mathbf{C}_f$ and $\mathbf{C}_i$ in a convolution sense [e.g.,

$$\int_0^T \int_\Omega \mathbf{W}_f(\mathbf{x}, t, \mathbf{x}', t') \mathbf{C}_f(\mathbf{x}', t', \mathbf{x}'', t'')\, d\mathbf{x}'\, dt' = \delta(\mathbf{x} - \mathbf{x}'') \delta(t - t'')$$

where $\delta$ denotes the Dirac delta function [see also Bennett (2002), p. 53], and $\mathbf{W}_\varepsilon$ is the matrix inverse of $\mathbf{C}_\varepsilon$. Boundary condition errors are omitted from (1) and (3) only for the sake of clarity. It has been shown in multiple publications related to variational data assimilation (e.g., Bennett 2002), that the solution of the assimilation problem [i.e., the minimization of the cost function in (3)], is achieved by solving the following Euler–Lagrange (EL) system,

$$\begin{cases} \dfrac{\partial \hat{\mathbf{u}}}{\partial t} = \mathbf{L}(\hat{\mathbf{u}}) + \mathbf{F} + \mathbf{C}_f \cdot \boldsymbol{\lambda}, & 0 \le t \le T, \\ \hat{\mathbf{u}}(\mathbf{x}, \mathbf{0}) = \mathbf{I}(\mathbf{x}) + \mathbf{C}_i \circ \boldsymbol{\lambda}(\mathbf{x}, 0), \\ -\dfrac{\partial \boldsymbol{\lambda}}{\partial t} = \left[\dfrac{\partial \mathbf{L}}{\partial \mathbf{u}}(\hat{\mathbf{u}})\right]^{\mathrm{T}} \boldsymbol{\lambda} + \displaystyle\sum_{m=1}^{M} \sum_{n=1}^{M} W_{\varepsilon,mn} (\mathbf{y}_m - \mathbf{H}_m \hat{\mathbf{u}}) \mathbf{H}_m^{\mathrm{T}} \delta(t - t_m), \\ \boldsymbol{\lambda}(\mathbf{x}, T) = 0, \end{cases} \tag{4}$$

where $\hat{\mathbf{u}}$ is the optimal solution, also referred to as the analysis, $\boldsymbol{\lambda}$ is the adjoint variable defined as the weighted residual:

$$\boldsymbol{\lambda}(\mathbf{x}, t) = \int_0^T \int_\Omega \mathbf{W}_f(\mathbf{x}, t, \mathbf{x}', t') \mathbf{f}(\mathbf{x}', t')\, d\mathbf{x}'\, dt', \tag{5}$$

and $W_{\varepsilon,mn}$ are the matrix elements of $\mathbf{W}_\varepsilon$, the superscript T denotes the transpose, and the covariance multiplication with the adjoint variable is the convolution:

$$\mathbf{C}_f \cdot \boldsymbol{\lambda}(\mathbf{x}, t) = \int_0^T \int_\Omega \mathbf{C}_f(\mathbf{x}, t, \mathbf{x}', t') \boldsymbol{\lambda}(\mathbf{x}', t')\, d\mathbf{x}'\, dt', \tag{6}$$

and

$$\mathbf{C}_i \circ \boldsymbol{\lambda}(\mathbf{x}, 0) = \int_\Omega \mathbf{C}_i(\mathbf{x}, \mathbf{x}') \boldsymbol{\lambda}(\mathbf{x}', 0)\, d\mathbf{x}', \tag{7}$$

for the model and initial condition errors, respectively. The convolution involved in (3), (5), (6), and (7) is written in a general form. However, the

definition of the covariance functions as in Ngodock and Carrier (2014a) gives this convolution its more familiar form.

Many applications of 4DVAR use the strong constraints assumption that errors are only present in the initial condition (i.e., $\mathbf{f} = 0$ or $\mathbf{C}_f$). As it is apparent in (4), the strong constraints assumption automatically neglects the dynamical contribution of the term $\mathbf{C}_f \cdot \boldsymbol{\lambda}(\mathbf{x}, t)$ to the correction of the model trajectory within the assimilation window. It is this contribution that we intend to substantiate using a linearized model.

### a. The representer method

We assume that the dynamical operator $\mathbf{L}$ has been linearized in some way and the model in (1) now takes the following form:

$$\begin{cases} \dfrac{\partial \mathbf{u}}{\partial t} = \mathbf{L}\mathbf{u} + \mathbf{F} + \mathbf{f}, & 0 \le t \le T, \\ \mathbf{u}(\mathbf{x}, 0) = \mathbf{I}(\mathbf{x}) + \mathbf{i}(\mathbf{x}). \end{cases} \tag{8}$$

The latter leads to a new EL system of the following form:

$$\begin{cases} \dfrac{\partial \hat{\mathbf{u}}}{\partial t} = \mathbf{L}\hat{\mathbf{u}} + \mathbf{F} + \mathbf{C}_f \cdot \boldsymbol{\lambda}, & 0 \le t \le T, \\ \hat{\mathbf{u}}(\mathbf{x}, 0) = \mathbf{I}(\mathbf{x}) + \mathbf{C}_i \circ \boldsymbol{\lambda}(\mathbf{x}, 0), \\ -\dfrac{\partial \boldsymbol{\lambda}}{\partial t} = \mathbf{L}^{\mathrm{T}}\boldsymbol{\lambda} + \displaystyle\sum_{m=1}^{M}\sum_{n=1}^{M} W_{\varepsilon,mn}(\mathbf{y}_m - \mathbf{H}_m\hat{\mathbf{u}})\mathbf{H}_m^{\mathrm{T}}\delta(t - t_m), \\ \lambda(x, T) = 0. \end{cases} \tag{9}$$

Without loss of generality, the EL system in (9) can be solved using the representer method (Bennett 1992, 2002), which expresses the optimal solution as the sum of a first guess $\mathbf{u}_F$ and a finite linear combination of representer functions $\mathbf{r}_m(\mathbf{x}, t)$, one per datum,

$$\hat{\mathbf{u}}(\mathbf{x}, t) = \mathbf{u}_F(\mathbf{x}, t) + \sum_{m=1}^{M} \beta_m \mathbf{r}_m(\mathbf{x}, t), \tag{10}$$

where $\beta_m$ are the representer coefficients. The first guess $\mathbf{u}_F$ is the solution of the model in (8) with no errors:

$$\begin{cases} \dfrac{\partial \mathbf{u}}{\partial t} = \mathbf{L}\mathbf{u} + \mathbf{F}, & 0 \le t \le T, \\ \mathbf{u}(\mathbf{x}, 0) = \mathbf{I}(\mathbf{x}), \end{cases} \tag{11}$$

and the representer function associated with the $m$th observation is the solution of the system:

$$\begin{cases} \dfrac{\partial \mathbf{r}_m}{\partial t} = \mathbf{L}\mathbf{r}_m + \mathbf{C}_f \cdot \boldsymbol{\alpha}_m, & 0 \le t \le T, \\ \mathbf{r}_m(\mathbf{x}, 0) = \mathbf{C}_i \circ \boldsymbol{\alpha}_m(\mathbf{x}, 0), \\ -\dfrac{\partial \boldsymbol{\alpha}_m}{\partial t} = \mathbf{L}^{\mathrm{T}}\boldsymbol{\alpha}_m + \mathbf{H}_m^{\mathrm{T}}\delta(t - t_m), \\ \boldsymbol{\alpha}_m(\mathbf{x}, T) = 0. \end{cases} \tag{12}$$

This system is fully uncoupled, since $\boldsymbol{\alpha}_m$, also referred to as the adjoint representer function, depends solely on the observation location and the dynamics of the adjoint model. Since the overall correction to the model solution is a linear combination of representer functions according to (10), it is thus sufficient to examine a single representer function in order to illustrate the difference between weak and strong constraints approaches.

### b. Single observation

The analytical solution for the adjoint representer in (12) is given by

$$\boldsymbol{\alpha}_m(t) = e^{-\int_{t_m}^{t} \mathbf{L}^{\mathrm{T}}(\mathbf{s})\, d\mathbf{s}} \Theta(t_m - t)\mathbf{H}_m^{\mathrm{T}}, \quad 0 \le t \le T, \tag{13}$$

where the space-independent variable $\mathbf{x}$ is omitted for the sake of clarity and $\Theta$ is the Heaviside step function:

$$\Theta(t) = \begin{cases} 1, & \text{if} \quad 0 \le t, \\ 0, & \text{if} \quad t < 0. \end{cases} \tag{14}$$

Substituting (13) into (12) gives

$$\mathbf{r}_m(t) = e^{\int_0^t \mathbf{L}(\mathbf{s})\, d\mathbf{s}} \left[ \int_0^t \mathbf{C}_f \circ e^{-\int_{t_m}^{t'} \mathbf{L}^{\mathrm{T}}(\mathbf{s})\, d\mathbf{s}} e^{-\int_0^{t'} \mathbf{L}(\mathbf{s})\, d\mathbf{s}} \Theta(t_m - t')\mathbf{H}_m^{\mathrm{T}}\, dt' + \mathbf{C}_i \circ \mathbf{H}_m^{\mathrm{T}} e^{-\int_{t_m}^{0} \mathbf{L}^{\mathrm{T}}(\mathbf{s})\, d\mathbf{s}} \right], \quad 0 \le t \le T. \tag{15}$$

It is clear from (15) that the difference between the strong and the weak constraints corrections is

$$\mathbf{e}_m(t) = e^{\int_0^t \mathbf{L}(\mathbf{s})\,d\mathbf{s}} \int_0^t \mathbf{C}_f \cdot e^{-\int_{t_m}^{t'} \mathbf{L}^{\mathrm{T}}(\mathbf{s})\,d\mathbf{s}} e^{-\int_0^{t'} \mathbf{L}(\mathbf{s})\,d\mathbf{s}} \Theta(t_m - t')\mathbf{H}_m^{\mathrm{T}}\,dt', \quad 0 \le t \le T. \tag{16}$$

This is the additional correction that can be extracted from the observation (and applied to the solution at times $t > 0$) but that is unfortunately thrown away with the strong constraints approach. We argue that (16) can be nonnegligible.

In general, the operator $\mathbf{L}$ can be decomposed into $\mathbf{L} = \mathbf{L}_G + \mathbf{L}_{\mathrm{NG}}$, where $\mathbf{L}_G$ and $\mathbf{L}_{\mathrm{NG}}$ represent the projections of $\mathbf{L}$ onto the two subspaces of its growing and nongrowing modes, respectively. The term $e^{\int_0^t \mathbf{L}(\mathbf{s})\,d\mathbf{s}}$ in (16) can be expanded into $e^{\int_0^t \mathbf{L}_G(\mathbf{s})\,d\mathbf{s}} e^{\int_0^t \mathbf{L}_{\mathrm{NG}}(\mathbf{s})\,d\mathbf{s}}$, where the first part grows with time and the second part decreases with time. Also, $e^{-\int_0^{t'} \mathbf{L}(\mathbf{s})\,d\mathbf{s}} = e^{-\int_0^{t'} \mathbf{L}_G(\mathbf{s})\,d\mathbf{s}} e^{-\int_0^{t'} \mathbf{L}_{\mathrm{NG}}(\mathbf{s})\,d\mathbf{s}}$ has a growing part associated with the nongrowing modes and a decreasing part associated with the growing modes, because of the negative sign of the exponent. This is also the case for $e^{-\int_0^{t'} \mathbf{L}^{\mathrm{T}}(\mathbf{s})\,d\mathbf{s}} = e^{-\int_0^{t'} \mathbf{L}_G^{\mathrm{T}}(\mathbf{s})\,d\mathbf{s}} e^{-\int_0^{t'} \mathbf{L}_{\mathrm{NG}}^{\mathrm{T}}(\mathbf{s})\,d\mathbf{s}}$. Thus, regardless of the stability of the operator $\mathbf{L}$, (16) will still grow with time. The presence of the operators $\mathbf{L}$ and $\mathbf{L}^{\mathrm{T}}$ ensures that the observation influence is propagated back and forth in space and time according to the dynamics of the tangent linear and adjoint models. This enables the weak constraints to allow more complex time dependence of the increment.

Note that in an actual assimilation the increments also depend on the representer coefficients, which in turn depend on the representer functions. Thus, the strong constraints representer coefficients will be different from their weak constraints counterpart. However, we argue that this difference in the magnitude of the coefficients is unable to help the strong constraint assimilation compensate for the loss of dynamical information contained in (16).

To examine whether the difference in (16) makes the weak constraints a better system than the strong constraints in terms of accuracy of the analysis, we carry out two comparison experiments: one using two single-observation assimilations, and the other involving all available observations in the selected domain and time window. Before delving into the experiments, it is important to note that in the absence of the model error term, the EL system in (4) becomes

$$\begin{cases} \dfrac{\partial \hat{\mathbf{u}}}{\partial t} = \mathbf{L}(\hat{\mathbf{u}}) + \mathbf{F}, & 0 \le t \le T, \\ \hat{\mathbf{u}}(\mathbf{x}, 0) = \mathbf{I}(\mathbf{x}) + \mathbf{C}_i \circ \boldsymbol{\lambda}(\mathbf{x}, 0), & \\ -\dfrac{\partial \boldsymbol{\lambda}}{\partial t} = \left[\dfrac{\partial \mathbf{L}}{\partial \mathbf{u}}(\hat{\mathbf{u}})\right]^{\mathrm{T}} \boldsymbol{\lambda} + \displaystyle\sum_{m=1}^{M} \sum_{n=1}^{M} W_{\varepsilon,mn}(\mathbf{y}_m - \mathbf{H}_m \hat{\mathbf{u}})\mathbf{H}_m^{\mathrm{T}} \delta(t - t_m), & \\ \boldsymbol{\lambda}(\mathbf{x}, T) = 0, & \end{cases} \tag{17}$$

which is usually solved iteratively, starting from a first-guess solution from which the model–data discrepancies are computed and used to solve that adjoint model. The latter is used to adjust the initial condition of the forward model that yields a new solution. The process is then repeated until formal convergence. It can be seen that for the choice of the first guess according to (11) the evolution of the correction to the model solution is given by the tangent linear model (TLM), just as with representer method. Thus, both the classic 4DVAR and the representer method would yield the same solution for the strong constraints approach as long as the TLM is stable and valid (i.e., the TLM propagates small initial perturbations linearly in time), and its solution closely matches the difference between two solutions of the nonlinear model with initial conditions that differ only by the initial perturbation (see also Errico et al. 1993).

## 3. Experiments and results

A comparison of how the strong and weak constraints approaches fit the observations is examined in two experiments: a single-observation assimilation for both SST and SSH, and the assimilation of all available observation within the model domain and the time interval selected. The assimilation system used for these experiments is the Navy Coastal Ocean Model (NCOM-4DVAR) described in Ngodock and Carrier (2014a). It is used here with a model setup for the Agulhas Current, in a domain that covers latitudes 25°–45°S and longitudes 0°–45°E. The model has a horizontal resolution of 10 km and a hybrid vertical coordinate that uses 25 sigma layers in the upper 125 m, and 25 $z$ levels from below the lowest sigma layer to the seafloor. Initial and lateral boundary conditions are taken from the global

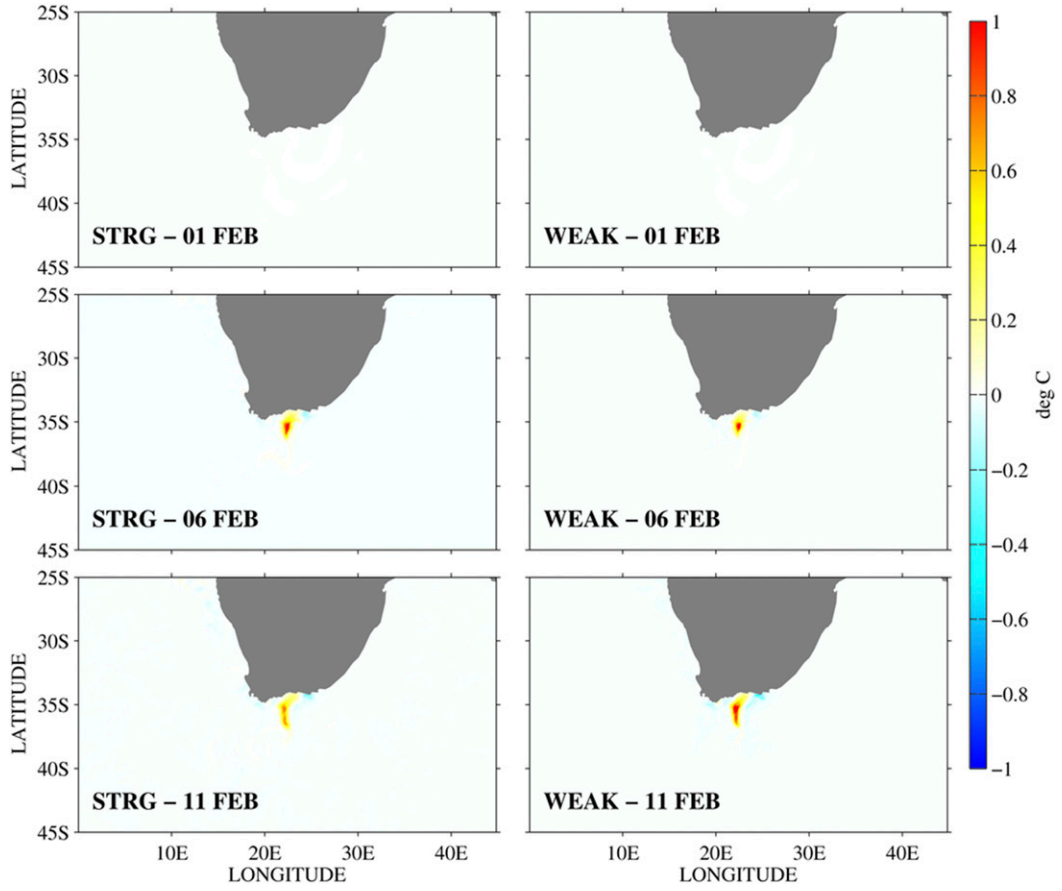


FIG. 1. Analysis increments from assimilating a single SST observation (°C) using (left) strong and (right) weak constraints at (top) day 0, the initial time, (middle) day 5, and (bottom) day 10.

solution of the NCOM (Barron et al. 2006), and atmospheric forcing fields are provided by the Navy Operational Global Atmospheric Prediction System (NOGAPS) of Rosmond et al. (2002) with a horizontal resolution of 0.5°. The NCOM-4DVAR system is run with the same covariances that were described in Ngodock and Carrier (2014b) for the errors in the observations, the initial conditions, and the model.

Two single-observation assimilation experiments are carried out separately for SST and SSH, respectively, in a 10-day window from 1 February to 11 February 2010. Both observations are located at 38°S, 24°E and day 5 of the 10-day window, and yield the respective positive innovations of 1°C and 1 m. The outcome of assimilating these single observations is examined through their respective increments, which should have the magnitude and sign of the innovations at the observation location.

### *a. Single SST observation*

Increments from the assimilation of the single SST observation are shown in Fig. 1 for both the strong and weak constraints, at the beginning (1 February), the middle (5 February), and the end (11 February) of the assimilation window. It can be seen that both strong and weak constraints have the same very small increment at the initial time. By day 5, the increments have grown yet remain similar in shape and magnitude. It should be noted that in the strong constraints, the growth of the increments is solely due to the propagation, through the tangent linear model, of the initial increment given by the adjoint model at the initial time. The weak constraints has the additional forcing from the adjoint model that, at least by day 5, does not seem to play a significant role. However, by day 10 the strong constraints SST increment has a lower magnitude than its weak constraint counterpart, although they both remain similar in shape. It is possible that the diffusion that is present in the model is affecting the strong constraint increment, while the weak constraint increment is able to maintain its magnitude due to the forcing from the adjoint.

### *b. Single SSH observation*

Similar to the assimilation of a single SST observation, increments from the assimilation of the single SSH

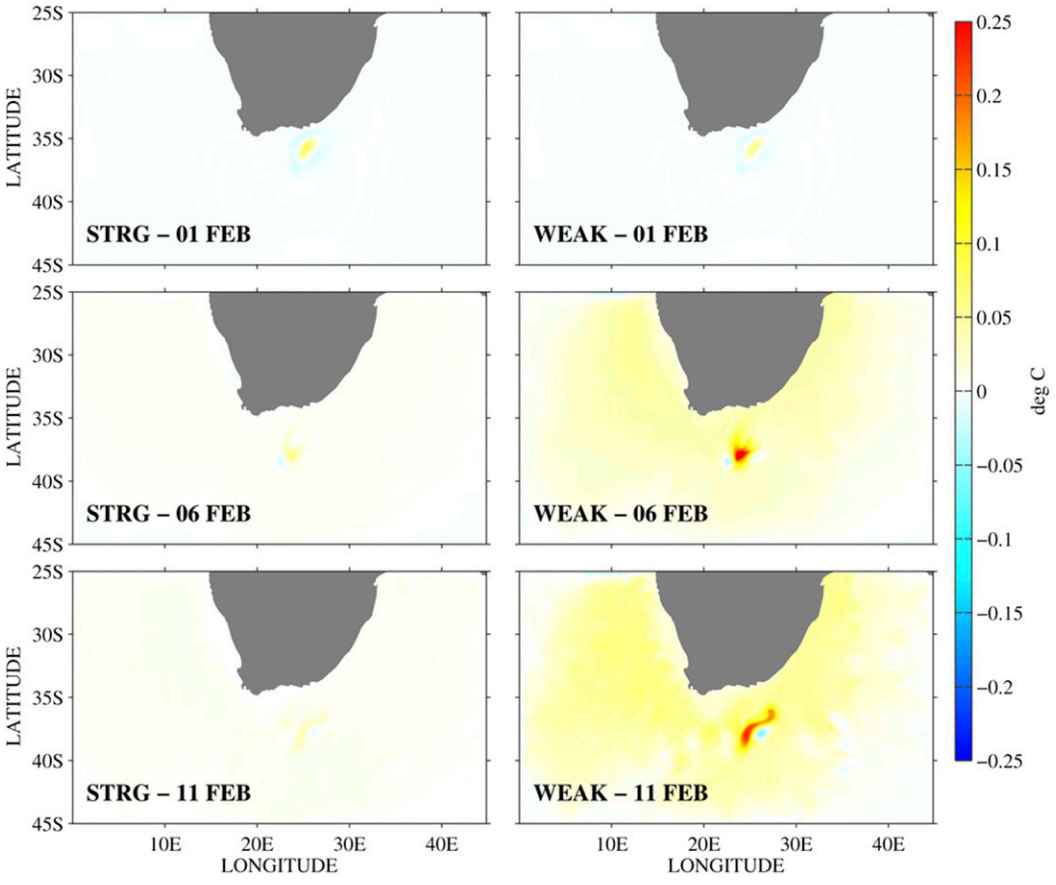


FIG. 2. As in Fig. 1, but for assimilating a single SSH observation.

observation are shown in Fig. 2 for both the strong and weak constraints, at the beginning (1 February), the middle (5 February), and the end (11 February) of the assimilation window. It can be seen that both strong and weak constraints have the same very small increment at the initial time. However, contrary to the single SST observation case, the strong constraint increment for SSH does not grow with time compared to its weak constraint counterpart; it actually decays. This is primarily due to the way SSH observations are assimilated in NCOM-4DVAR (see Ngodock et al. 2016), in addition to the adjoint forcing in the weak constraint. Figure 2 illustrates the contribution of (16) above in helping the weak constraint to produce a meaningful increment, especially when the observation is distant from the initial time.

### c. *Multiobservations*

The third experiment consists of assimilating a set of real observations from GOES and AVHRR for SST, *Jason-2* altimeter (interleaved) for SSH, and temperature and salinity profiles from the Argo floats. The summation involved in (10) suggests that for a full set of observations there will be an aggregation of the differences in (16) (illustrated with the assimilation of single observation), even though all representer coefficients in (10) may not be positive or have the same magnitude. The significant difference seen in the case of the assimilation of a single SSH observation indicated that the weak constraint is better suited for fitting SSH observations. Along-track SSH analysis residuals are shown in Fig. 3, in a comparison of the free run (no assimilation), the strong and the weak constraints at three different 10-day windows: 21 February–3 March, 22 April–2 May, and 21 June–1 July. The free-run solution is included in this comparison to highlight the marked improvements (reduction of prior observations–model discrepancies–misfits) of the strong constraints, especially in the Benguela, the Agulhas leakage, retroflection, and return current regions. The analysis residuals are significantly lower in the weak than in the strong constraints. This result illustrates that (16) contributes to better fitting the observations.

### d. *Fit to the observations*

A metric that defines the fit to the observations in the whole assimilation window is given by

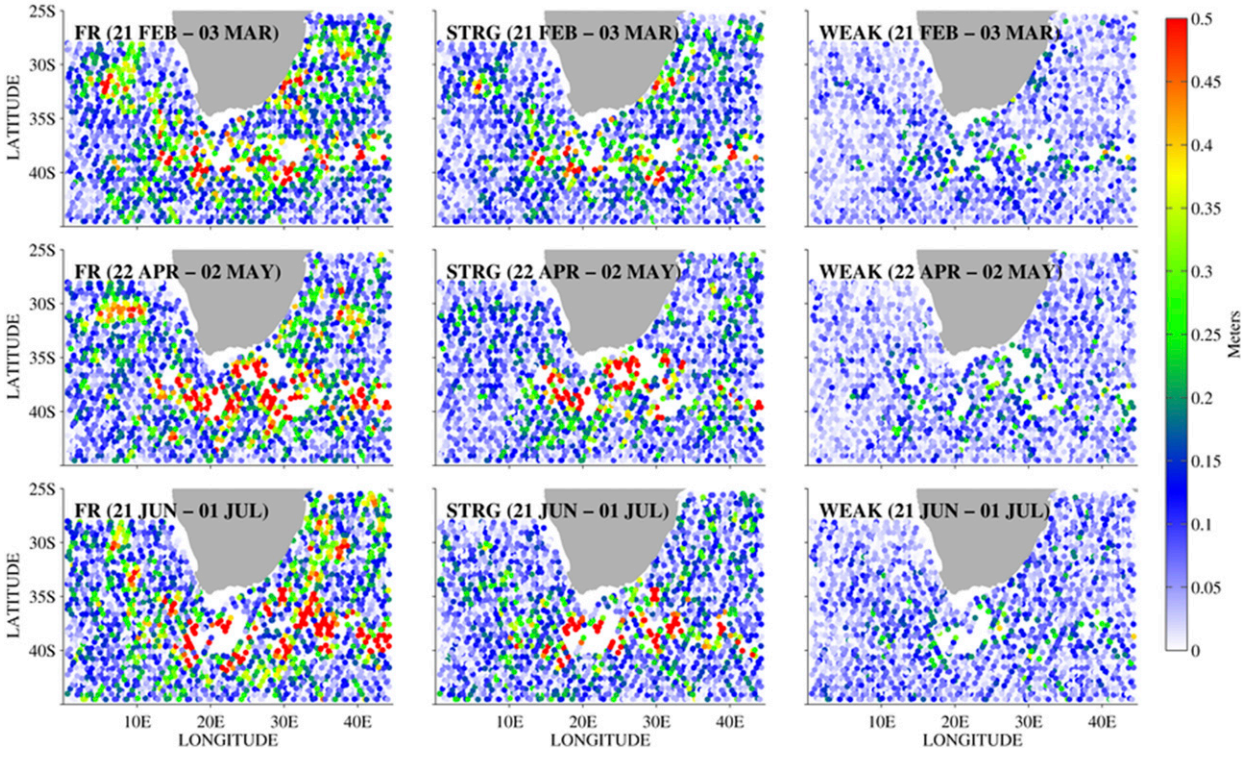


FIG. 3. Along-track SSH (m) analysis residuals from the (left) free run, and the (middle) strong and (right) weak constraints assimilations for three 10-day windows: (top) 21 Feb–3 Mar, (middle) 22 Apr–2 May, and (bottom) 21 Jun–1 Jul.

$$J = \frac{1}{M}\sum_{m=1}^{M}\frac{|\mathbf{y}_m - \mathbf{H}_m\mathbf{u}|}{\sigma_m}, \tag{18}$$

where $\mathbf{y}_m$ is the $m$th observation, $M$ is the total number of observations, $\mathbf{H}_m$ is the $m$th observation operator, $\mathbf{u}$ is the model solution, and $\sigma_m$ is the observation error or standard deviation. The right-hand side of (18) can be computed as a time series, for the analysis $\hat{\mathbf{u}}$ ($J_{\mathrm{FIT}}$), the free-run solution $\mathbf{u}_F$ ($J_{\mathrm{FREE}}$), and the first-guess $\mathbf{u}_{\mathrm{FG}}$ ($J_{\mathrm{FG}}$). The first guess is a series of 10-day forecast solutions that is initialized by the analysis at the end of every assimilation cycle. Since both the free run and the first guess are predicted solutions, $J_{\mathrm{FREE}}$ and $J_{\mathrm{FG}}$ are also collectively referred to as $J_{\mathrm{PRED}}$. The values of $J_{\mathrm{FIT}}$, $J_{\mathrm{FREE}}$, and $J_{\mathrm{FG}}$ represent the number of observation error standard deviation by which the respective solutions depart from the observations. They are shown in Fig. 4 (as a time series) for surface and subsurface temperature (left panels), and SSH (right panels). For the sake of clarity $J_{\mathrm{FIT}}$ (top) and $J_{\mathrm{PRED}}$ (bottom) are shown in separate panels, where $J_{\mathrm{FIT}}$ comprises both the strong and weak constraints analyses. Since the assimilation is expected to fit the observations to within the observation at the observation locations, the metric $J_{\mathrm{FIT}}$ in (18) is expected to be less or equal to 1 for the analysis. There is no such expectation for $J_{\mathrm{PRED}}$ as a result of fitting the observations in previous cycles. However, it is assumed that since the forecast is started from a better initial condition (the analysis at the end of the previous assimilation cycle), it should yield a solution that is closer to the observations than the free run (i.e., $J_{\mathrm{FG}}$ should have lower values than $J_{\mathrm{FREE}}$).

It can be seen in Fig. 4 that the free run does not agree with the observations at all, having values that generally fluctuate between 3 and 4 for SSH, and between 2 and 3 for temperature. The first guess has lower $J_{\mathrm{PRED}}$ values than the free run, with more noticeable improvements in temperature than SSH. Also, the first guess from the weak constraint generally has lower $J_{\mathrm{PRED}}$ values than the first guess from the strong constraint. For temperature, the $J_{\mathrm{PRED}}$ values for the first guess are around 1.5 (2) for the weak (strong) constraints, and for SSH the values fluctuate between 2 and 2.5 (2 and 3.5) for the weak (strong) constraints. Thus, there is not much improvement in SSH from the free run to the strong constraint first guess. It is the $J_{\mathrm{FIT}}$ values for the assimilated solutions that show the superior ability of the weak constraint to fit the observations compared to the strong constraint; they are around 1 (1 to 1.5) for temperature

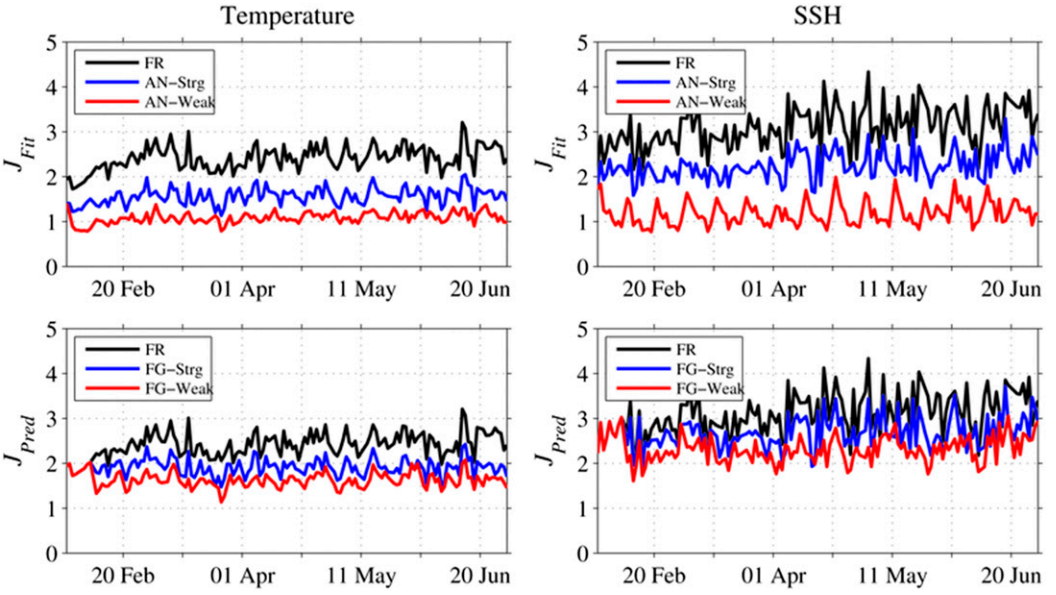


FIG. 4. Time series of the fit to the observations metric for (top) the analysis and (bottom) the forecast, computed for (left) temperature and (right) SSH. The free-run solution is in black and the strong and weak constraints assimilations are in blue and red, respectively.

(SSH) in the weak constraint, and around 1.5 (2 to 2.5) for temperature (SSH) in the strong constraint, over the entire 5-month assimilation period.

The assimilation process is a generalized inversion that can be used as a significance test of the hypothesized prior statistics for the errors. It has been shown (e.g., Bennett 1992) that if the initial conditions, model, and observations errors are unbiased and not mutually correlated, and are Gaussian with the prescribed covariances for a linear problem, then the minimized cost function ($J_{\mathrm{MIN}}$) is a chi-squared random variable with $M$ degrees of freedom (i.e., its mean is $M$ and its variance is $2M$, $M$ being the number of assimilated observations). The value of the $J_{\mathrm{MIN}}$ is computed after each assimilation cycle and normalized by $M$, then used to evaluate both strong and weak constraints assimilations. Note that because $M$ can vary from one assimilation cycle to another, the normalization of $J_{\mathrm{MIN}}$ by $M$ ensures that the mean and variance of the normalized $J_{\mathrm{MIN}}$ should be 1 and $2/M$ regardless of $M$.

It can be seen in Fig. 5 that both the strong and weak constraints assimilations fail the significance test: the weak and strong constraints values fluctuate around 2 and 3 times their expected mean, respectively. It is arguably a difficult task to prescribe error statistics for which the assimilation system satisfies that significance test. However, although having values that are significantly higher that its expected mean, the weak constraints $J_{\mathrm{MIN}}$ is still significantly closer to 1 than its strong constraints counterpart. Thus, the added degrees of freedom through the model error in the weak constraints enable it to be more likely to satisfy the significance test than the strong constraints.

## 4. Discussion

There is a tendency in these years to abandon the variational approach in favor of ensemble-based assimilation methods for the main reasons that the adjoint model is tedious to develop, and both the TLM and adjoint may not be stable, and they have to be maintained if the model is modified (Kalnay et al. 2007; Gustafsson 2007; Yaremchuk et al. 2009; Zheng et al. 2016). More and more hybrid approaches are being proposed, as well as adjoint-free methods (Zheng et al. 2016).

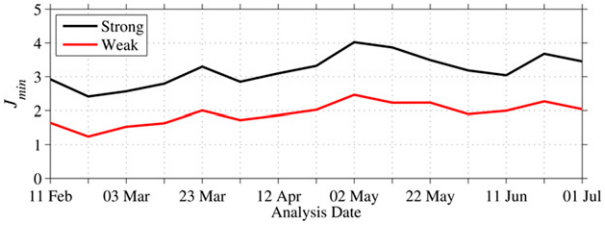


FIG. 5. Time series of normalized $J_{\mathrm{MIN}}$ values for each assimilation cycle. The strong and weak constraints assimilations are in black and red, respectively.

In general, these considerations are based on the conclusions drawn from strong constraints 4DVAR applications (see Skachko et al. 2014). We argue that the weak constraints formulation is a viable 4DVAR option that provides superior results compared to the strong constraints. In addition, with the modular approach adopted in contemporary numerical models, the adjoint model is no longer difficult to maintain: changes and upgrades to models are typically implemented within a few modules, and thus only the adjoint of those modules need to be upgraded. Also, there exist tools for automatic generation of computer codes for tangent linear and adjoint of numerical models (e.g., Giering and Kaminski 2003; Vlasenko et al. 2016). Furthermore, the computational cost of the weak constraints 4DVAR, which is usually touted as another drawback, can be significantly reduced by using the representer method equipped with 1) a suitable preconditioner (e.g., Gratton and Tshimanga 2009), and 2) an efficient implementation of the model error covariance multiplication (Ngodock 2005). With these two implementations the weak constraints 4DVAR uses only a few more iterations (one to three) than the strong constraints 4DVAR, and each iteration of the weak constraints is only slightly more computationally expensive than a strong constraints iteration.

## 5. Conclusions

The difference between the strong and weak constraints 4DVAR analyses is examined using the representer method formulation, which expresses the analysis as the sum of a first guess and a finite linear combination of representer functions. The latter are computed analytically for a single observation in both strong and weak constraints assumptions. It is argued that although the final increments depend on both the representer functions and the representer coefficients, the latter also depend on the representer functions. Thus, even though the strong constraints representer coefficients are different from their weak constraints counterpart (due to the difference in the respective representer functions), that difference is unable to help the strong constraints compensate the loss of information expressed in (16). Numerical experiments were carried out in the Agulhas retroflection for a single SST, a single SSH observation, and multiobservations assimilations, using the NCOM-4DVAR system. Results clearly show that the weak constraint 4DVAR produces analyses that fit the observations with significantly higher accuracy than the strong constraints. The superior accuracy is also seen in the resulting forecasts, although not as significant as in the analyses. The representer formulation allows us to solve the weak constraint 4DVAR problem at just a slightly higher computational cost than the strong constraints.

*Acknowledgments.* This work was sponsored by the Office of Naval Research Program Element 0601153N as part of the ''Coupled Ocean–Atmosphere 4DVAR'' project. The authors thank the anonymous reviewers for their constructive comments that helped to improve the quality of the manuscript.

## REFERENCES

Barron, C. N., A. B. Kara, P. J. Martin, R. C. Rhodes, and L. F. Smedstad, 2006: Formulation, implementation and examination of vertical coordinate choices in the Global Navy Coastal Ocean Model (NCOM). *Ocean Modell.*, **11**, 347–375, doi:10.1016/j.ocemod.2005.01.004.

Bennett, A. F., 1992: *Inverse Methods in Physical Oceanography*. Cambridge University Press, 368 pp.

——, 2002: *Inverse Modeling of the Ocean and Atmosphere.* Cambridge University Press, 234 pp.

Courtier, P., J.-N. Thepaut, and A. Hollingsworth, 1994: A strategy for operational implementation of 4D-Var, using an incremental approach. *Quart. J. Roy. Meteor. Soc.*, **120**, 1367–1387, doi:10.1002/qj.49712051912.

Di Lorenzo, E., A. M. Moore, H. G. Arango, B. D. Cornuelle, A. J. Miller, B. Powell, B. S. Chua, and A. F. Bennett, 2007: Weak and strong constraint data assimilation in the inverse Regional Ocean Modeling System (ROMS): Development and application for a baroclinic coastal upwelling system. *Ocean Modell.*, **16**, 160–187, doi:10.1016/j.ocemod.2006.08.002.

Errico, R. M., T. Vukicevic, and K. Raeder, 1993: Examination of the accuracy of a tangent linear model. *Tellus*, **45A**, 462–477, doi:10.1034/j.1600-0870.1993.00010.x.

Giering, R., and T. Kaminski, 2003: Applying TAF to generate efficient derivative code of Fortran 77–95 programs. *Proc. Appl. Math. Mech.*, **2**, 54–57, doi:10.1002/pamm.200310014.

Gratton, S., and J. Tshimanga, 2009: An observation-space formulation of variational assimilation using a restricted preconditioned conjugate gradient algorithm. *Quart. J. Roy. Meteor. Soc.*, **135**, 1573–1585, doi:10.1002/qj.477.

Gustafsson, N., 2007: Discussion on '4D-Var or EnKF?' *Tellus*, **59A**, 774–777, doi:10.1111/j.1600-0870.2007.00262.x.

Kalnay, E., H. Li, T. Miyoshi, S.-C. Yang, and J. Ballabrera-Poy, 2007: 4D-Var or Ensemble Kalman Filter? *Tellus*, **59A**, 758–773, doi:10.1111/j.1600-0870.2007.00261.x.

Le Dimet, F-X., and O. Talagrand, 1986: Variational algorithms for analysis and assimilation of meteorological observations: Theoretical aspects. *Tellus*, **38A**, 97–110.

Lindskog, M., D. Dee, Y. Trémolet, E. Andersson, G. Radnóti, and M. Fisher, 2009: A weak-constraint four-dimensional variational analysis system in the stratosphere. *Quart. J. Roy. Meteor. Soc.*, **135**, 695–706, doi:10.1002/qj.392.

Ngodock, H., 2005: Efficient implementation of covariance multiplication for data assimilation with the representer method. *Ocean Modell.*, **8**, 237–251, doi:10.1016/j.ocemod.2003.12.005.

——, and M. Carrier, 2014a: A 4DVAR system for the Navy Coastal Ocean Model. Part I: System description and

assimilation of synthetic observations in Monterey Bay. *Mon. Wea. Rev.*, **142**, 2085–2107, doi:10.1175/MWR-D-13-00221.1.

——, and ——, 2014b: A 4DVAR system for the Navy Coastal Ocean Model. Part II: Strong and weak constraint assimilation experiments with real observations in Monterey Bay. *Mon. Wea. Rev.*, **142**, 2108–2117, doi:10.1175/MWR-D-13-00220.1.

——, ——, I. Souopgui, S. R. Smith, P. Martin, P. Muscarella, and G. A. Jacobs, 2016: On the direct assimilation of along-track sea-surface height observations into a free-surface ocean model using a weak constraints four-dimensional variational (4D-Var) method. *Quart. J. Roy. Meteor. Soc.*, **142**, 1160–1170, doi:10.1002/qj.2721.

Rosmond, T. E., J. Teixeira, M. Peng, T. F. Hogan, and R. Pauley, 2002: Navy Operational Global Atmospheric Prediction System (NOGAPS): Forcing for ocean models. *Oceanography*, **15**, 99–108, doi:10.5670/oceanog.2002.40.

Skachko, S., Q. Errera, R. Ménard, Y. Christophe, and S. Chabrillat, 2014: Comparison of the ensemble Kalman filter and 4D-Var assimilation methods using a stratospheric tracer transport model. *Geosci. Model Dev.*, **7**, 1451–1465, doi:10.5194/gmd-7-1451-2014.

Vidard, P. A., A. Piacentini, and F.-X. LeDimet, 2004: Variational data analysis with control of the forecast bias. *Tellus*, **56A**, 177–188, doi:10.1111/j.1600-0870.2004.00057.x.

Vlasenko, A. V., A. Köhl, and D. Stammer, 2016: The efficiency of geophysical adjoint codes generated by automatic differentiation tools. *Comput. Phys. Commun.*, **199**, 22–28, doi:10.1016/j.cpc.2015.10.008.

Yaremchuk, M., D. Nechaev, and G. Panteleev, 2009: A method of successive corrections of the control subspace in the reduced-order variational data assimilation. *Mon. Wea. Rev.*, **137**, 2966–2978, doi:10.1175/2009MWR2592.1.

Zheng, X., R. Mayerle, Q. Qianguo Xing, and J. M. F. Jaramillo, 2016: Adjoint free four-dimensional variational data assimilation for a storm surge model of the German North Sea. *Ocean Dyn.*, **66**, 1037–1050, doi:10.1007/s10236-016-0962-y.

Zupanski, D., 1997: A general weak constraint applicable to operational 4DVAR data assimilation systems. *Mon. Wea. Rev.*, **125**, 2274–2292, doi:10.1175/1520-0493(1997)125<2274:AGWCAT>2.0.CO;2.